DOI 10.5012/bkcs.2011.32.8.2765

The Concentration-Dependent Distribution of Tris(4,7'-diphenyl-1,10'-phenanthroline) Ruthenium (II) within Sol-Gel-Derived Thin Films

Joo-Woon Lee and Eun Jeong Cho[†,*]

Chemistry-School of Liberal Arts and Sciences, Chungju National University, Chungbuk 380-702, Korea
[†]*The Texas Institute for Drug and Diagnostic Development, The University of Texas at Austin, Austin, TX, 78712, USA*
[*]*E-mail: euncho@mail.utexas.edu*
Received May 27, 2011, Accepted July 8, 2011

Organic dye-doped glasses, *viz.*, ruthenium (II) tris(4,7'-diphenyl-1,10'-phenanthroline) $[Ru(dpp)_3]^{2+}$ incorporated into thin silica xerogel films produced by the sol-gel method, were prepared and their O_2 quenching properties investigated as a function of the $[Ru(dpp)_3]^{2+}$ concentration (3-400 μM) within the xerogel. The ratio of the luminescence from the $[Ru(dpp)_3]^{2+}$-doped films in the presence of N_2 and O_2 (I_{N2}/I_{O2}) was used to describe the film sensitivity to O_2 quenching. I_{N2}/I_{O2} changed three-fold over the $[Ru(dpp)_3]^{2+}$ concentration range. Time-resolved intensity decay studies showed that there are two discrete $[Ru(dpp)_3]^{2+}$ populations within the xerogels ($\tau_1 \sim 300$ ns; $\tau_2 \sim 3000$ ns) whose relative fraction changes as the $[Ru(dpp)_3]^{2+}$ concentration changes. The increased O_2 sensitivity that is observed at the higher $[Ru(dpp)_3]^{2+}$ concentrations is a manifestation of a greater fraction of the 3000 ns $[Ru(dpp)_3]^{2+}$ species (more susceptible to O_2 quenching). A model is presented to describe the observed response characteristics resulting from $[Ru(dpp)_3]^{2+}$ distribution within the xerogel.

Key Words : Ru(II) dopant, Sol-gel, Luminescence, Optical sensor

Introduction

Sol-gel processing is an attractive method that can be used to prepare a variety of novel materials that contain a wide range of active dopants (e.g., catalysts, chromophores, recognition chemistries, and proteins).[1-7] Over the past decade, sol-gel-processed thin films have been used in concert with a number of Ru(II) tris α-diimine dopants to produce luminescence-based sensors for O_2 quantification, with potential clinical, environmental, and process control applications.[8-11] Particularly promising among the Ru(II) diimine series is tris(4,7'-diphenyl-1,10'-phenanthroline) Ru(II) ($[Ru(dpp)_3]^{2+}$) which exhibits a high luminescence quantum yield, a long-lived excited-state luminescence lifetime, good photostability, large emission Stokes shift, and high molar absorptivity in the blue-green spectral region.[12-17] The photophysics and photochemistry of Ru(II) diimine quenching by O_2 is also well understood.[18-20]

There have been a few studies on the behavior of Ru(II) diimines when they are sequestered within sol-gel-derived glasses. For example, Knobbe and co-workers investigated the behavior of tris(2,2'-bipyridyl)ruthenium (II) chloride ($[Ru(bpy)_3]^{2+}$) sequestered within silica, acrylate, and epoxide hosts as the initial $[Ru(bpy)_3]^{2+}$concentration was varied from 0.7-100 mM.[21] These authors found that the emission spectra, luminescence quantum yields, and average excited-state luminescence lifetimes depended on the host matrix and on the $[Ru(bpy)_3]^{2+}$ concentration within the xerogel. Baker *et al.*[22] reported on the effects of xerogel processing temperature on the luminescence from $[Ru(dpp)_3]^{2+}$ (concentration fixed at 200 μM) sequestered within tetraethylorthosilane (TEOS) based xerogels. These experiments demonstrated that there is a dramatic increase in O_2 sensitivity when the $[Ru(dpp)_3]^{2+}$-doped films are processed at elevated temperatures. The increased sensitivity arose because there are two main types of $[Ru(dpp)_3]^{2+}$ microenvironments within the xerogel and higher temperature curing leads to an increase in the bimolecular quenching rate between O_2 and $[Ru(dpp)_3]^{2+}$.

In this paper we aim to determine how the $[Ru(dpp)_3]^{2+}$ concentration, within TEOS-derived thin films, affects the sensitivity of these films to O_2 and establish the origin of the observed changes in the film sensitivity to O_2 as the $[Ru(dpp)_3]^{2+}$ concentration within the film is adjusted.

Theory

The best description of luminophore quenching by a quencher like O_2 depends on the luminophore distribution within the host matrix and the total fraction of all luminophore molecules that occupy individual or ensembles of sites and/or domains within the host matrix.[22] If the time-resolved intensity decay kinetics from an unquenched luminophore is described by a single exponential decay law, purely dynamic O_2-induced luminophore quenching will obey the classic form of the Stern-Volmer relationship:[23]

$$\frac{I_0}{I} = \frac{\tau_0}{\tau} = 1 + K_{SV} pO_2 = 1 + k_q \tau_0 pO_2 \quad (1)$$

where I_0 and I are the steady-state luminescence intensities in the absence and presence of O_2, τ_0 and τ are the excited-state luminescence lifetimes in the absence and presence of

O_2, pO_2 is the O_2 partial pressure, K_{SV} is the dynamic Stern-Volmer quenching constant, and k_q is the bimolecular rate constant describing the efficiency of the collisional encounters between the luminophore and the quencher. For this ideal case, a plot of I_0/I or τ_0/τ versus pO_2 will be linear with a slope equal to K_{SV} and an intercept of unity.

If we consider a more complex host matrix, where the ensemble of luminescent species within the matrix encounter different environmental influences on an averaged time scale, the luminophores may exhibit characteristic quenching constants that can be associated with *each* distinct luminophore site and/or location within the host matrix. Such a consideration is appropriate where a few discrete luminophore microdomains or multiple interaction types are expected *a priori* as in cases involving ground-state heterogeneity (e.g., solid-state matrices, interfacial adsorption etc.). In this scenario, the overall Stern-Volmer expression is simply the superposition over all sites and eq. (1) can be recast as:

$$\frac{I_0}{I} = \frac{\langle \tau_0 \rangle}{\langle \tau \rangle} = \left[\sum_{i=1}^{m} \frac{f_i}{1 + K_{sv,i} pO_2} \right]^{-1} \quad (2)$$

for a system comprised of m luminophore microdomains where f_i denotes the fractional contribution to the i^{th} component, $K_{SV,i}$ is the Stern-Volmer quenching constant associated with the i^{th} component, and all other terms are as described above. Such a representation is likely for the present work given the ample precedent for heterogeneous microdomains surrounding dopants sequestered within xerogels.[24]

In a multisite model, the luminophore time-resolved intensity decay kinetics are best described by:

$$I(t) = \sum_{i=1}^{m} \alpha_i e^{-t/\tau_i} \quad (3)$$

In this expression, $I(t)$ represents the excited-state luminescence intensity decay following δ-pulse excitation, α_i denotes the pre-exponential amplitude associated with the i^{th} component, τ_i is the excited-state luminescence lifetime of the i^{th} component, and m is the number of discrete single-exponential components required to sufficiently describe the intensity decay kinetics.

If one recasts eq. (2) for the special case where $m = 2$, one has the familiar "two-site" model commonly used by Demas and co-workers:[15,25]

$$\frac{I_0}{I} = \frac{\tau_0}{\tau} = \left[\frac{f_1}{1 + K_{SV1} pO_2} + \frac{f_2}{1 + K_{SV2} pO_2} \right]^{-1} \quad (4)$$

In this expression, f_i denotes the fractional contribution of the total emission from the luminophore located at site type i under unquenched conditions that exhibits a discrete Stern-Volmer quenching constant given by K_{SVi}. In its simplest embodiment, such a representation is mathematically equivalent to a biexponential decay of $I(t)$ where each component independently fulfills a classic Stern-Volmer relationship.

Experimental Section

Chemical Reagents. Tris(4,7'-diphenyl-1,10'-phenanthroline) ruthenium(II) chloride pentahydrate ($[Ru(dpp)_3]^{2+}$, see Figure 2 inset for structure) was purchased from GFS Chemicals, Inc. and purified as described in the literature.[17] Tetraethylorthosilane (TEOS) was purchased from United Chemical Technologies, hydrochloric acid was obtained from Fisher Scientific Co., and EtOH was a product of Quantum Chemical Corp.. All reagents were used as received without further purification.

Preparation of $Ru(dpp)_3^{2+}$-Doped Sol-gel-Derived Thin Films. An acid-catalyzed sol-gel-processed stock solution was prepared by mixing TEOS (3.345 mL, 15 mmole), deionized water (0.54 mL, 30 mmole), EtOH (1.70 mL, 30 mmole), and HCl (15 μL of 0.1 M HCl, 15×10^{-4} mmole). This solution was stirred under ambient conditions for 4 h. We then took this mixture and transferred 700 μL aliquots into a series of seven (7) clean glass vials. To six (6) of the vials we then added 50 μL of $[Ru(dpp)_3]^{2+}$ dissolved in EtOH. To the seventh vial (the blank) we added 50 μL of EtOH. The ethanolic $[Ru(dpp)_3]^{2+}$ solutions contained 2.12, 7.43, 37.1, 74.4, 146.5, or 297.5 μmoles of $Ru(dpp)_3^{2+}$. The final $[Ru(dpp)_3]^{2+}$ concentration within these seven vials was thus 0, 3, 10, 50, 100, 200, or 400 μM. These solutions were allowed to stir for 1 h.

Films were all prepared on glass substrates. Toward this end, we cleaned a set of 2.5 × 2.5 cm glass microscope slides by soaking them in 1 M KOH for 4 h. These microscope slides were then rinsed with copious amounts of deionized water and EtOH and dried in an oven at 80 °C for 4 days. Films were spin cast (2000 rpm, 30 s) onto the glass surfaces as described elsewhere.[26] The xerogel film thickness was 0.9 ± 0.1 μm. Following this deposition step, all films were initially aged under ambient conditions for 7 days. Two of each film type were then soaked in 10 mL of EtOH under ambient conditions for 4 days and then rinsed with copious amounts of distilled-deionized water and EtOH. These soaked films were then allowed to dry under ambient conditions for 2 days and then dried further at 80 °C for 24 h. The films that were not soaked in EtOH were allowed to age under ambient conditions for 6 additional days (13 days total) and were then aged at 80 °C for 24 h. All films were allowed to cool to room temperature before spectroscopic measurements. Films that were soaked in EtOH are referred to as "soaked" films and those films that were not subjected to EtOH are denoted as "original" films.

All experiments were performed in triplicate using different reagent batches. Results are reported as the average of all measurements. All measurement imprecision represents ± one standard deviation.

Instrumentation. All steady-state fluorescence measurements were carried out using a SLM-Aminco Model 48000 MHF spectrofluorometer. A xenon arc lamp was used as the excitation source (450 nm). Emission spectra and slow-time acquisition were obtained using a monochromator for wavelength selection with photomultiplier tube detection. The

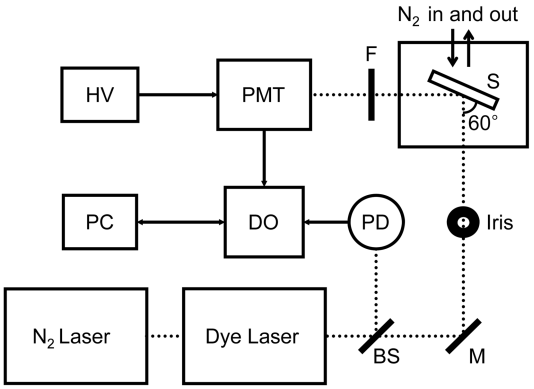

Figure 1. Simplified schematic of the instrumental setup used to record the time-resolved luminescence decay profiles. Abbreviations are: BS, beam splitter; M, mirror; PD, photodiode; PMT, photomultiplier; DO, digital-sampling oscilloscope; PC, personal computer; F, 640 nm bandpass filter; S, sample; HV, high voltage power supply.

excitation and emission bandpasses were set at 8 and 4 nm, respectively. The excitation radiation impinged on the film-coated side of the glass substrates at an incident angle of ~60° with a 90° angle maintained between the excitation beam trajectory and the emission collection optics.

To monitor the performance of the $Ru(dpp)_3^{2+}$-doped xerogel films we monitored the emission (570 nm long pass filter) as we cycled the environment surrounding the sample between N_2 and O_2.

Figure 1 shows a simplified schematic of the instrumental setup that we used to perform the time-resolved intensity decay measurements. The system consists of a dye laser (Photon Technology International, Model GL-301) that is pumped by a N_2-laser (Photon Technology International, Model GL-3300). The dye laser output is adjusted to 441 nm, and it produces 500 ps pulses at a repetition rate of 5-10 Hz. A small fraction of the laser beam output is directed to a photodiode (PD) which serves to trigger a 200 MHz digital oscilloscope (DO) (Tekronix, Model TDS 350). The remainder of the laser beam is reflected from a mirror (M) and passed through an iris that is used to control the excitation beam fluence at the sample (S) film surface. The emission from the film is filtered through a 640 nm interference filter (11 nm bandpass) (F) to prevent the excitation radiation from reaching the detector and detected by using a photomultiplier tube (PMT, Hammamatsu model R928) that is operated at −1000 V DC (HV). The PMT anode output is directed to the DO and terminated into 50 Ω. The DO output is sent to a personal computer (PC). During the measurement, N_2 was used to purge the sample chamber and data was only collected when the area under the decay profile was constant to within ± 2%. A CVI LabWindows software program is used to acquire the data and software from SigmaPlot was used to recover the kinetic terms from the time-resolved intensity decay profiles.

Results and Discussion

Steady-State Luminescence Measurements. The luminescence from $[Ru(dpp)_3]^{2+}$-doped sol-gel derived thin film arises from de-excitation from an excited-state triplet metal-to-ligand charge transfer[3] (MLCT) transition back to the ground singlet state.[27] The normalized excitation and emission spectra from our $[Ru(dpp)_3]^{2+}$-doped sol-gel-derived thin films were independent of the $[Ru(dpp)_3]^{2+}$ concentration (results not shown). The excitation and emission maxima were seen at 450 ± 3 nm and 580 ± 4 nm. These results argue that the $[Ru(dpp)_3]^{2+}$ concentration, over the range studied, does not affect the $[Ru(dpp)_3]^{2+}$ spectral profiles. This is in contrast to the results reported for $[Ru(bpy)_3]^{2+}$ between 0.7 and 100 mM.[21]

$[Ru(dpp)_3]^{2+}$-Doped Film Response to O_2 and N_2 Cycling. The observed response time of the films to O_2 and N_2 were a function of the $[Ru(dpp)_3]^{2+}$ concentration. In general, as the $[Ru(dpp)_3]^{2+}$ concentration decreased, the response time (time to reach 90% of the steady-state signal) increased. For example, the response time to O_2 for a 400 μM $[Ru(dpp)_3]^{2+}$ film was ~1 s whereas the response time was ~30 s for identically prepared/processed films that contained less than 10 μM $[Ru(dpp)_3]^{2+}$. This result suggests that the $[Ru(dpp)_3]^{2+}$ is distributing in a concentration-dependent manner within the xerogel films. Those films that were soaked in EtOH exhibited a statistically relevant (10-15%) increase in the response time compared to the original films. This result suggests that the EtOH soaking step removes the more accessible (i.e., weakly adsorbed) $[Ru(dpp)_3]^{2+}$ molecules from within the xerogel.

Figure 2 presents the ratio of the luminescence in the presence of N_2 and O_2 (I_{N2}/I_{O2}) for the $[Ru(dpp)_3]^{2+}$-doped sol-gel derived thin films as a function of $[Ru(dpp)_3]^{2+}$ concentration and film treatment. These results show several interesting features. First, the I_{N2}/I_{O2} ratio decreases (i.e., the sensitivity to O_2 decreases) when the films are soaked in EtOH. This result argues that the EtOH soaking step removes some of the more accessible $[Ru(dpp)_3]^{2+}$ species from the xerogel pore surface. ($[Ru(dpp)_3]^{2+}$ is observed in the EtOH soaking solution, but the amount is generally) Second, there is a general decrease in I_{N2}/I_{O2} as the $[Ru(dpp)_3]^{2+}$ concentration in the film decreases. (The value for the 3 μM "original" film is somewhat anomalous, but the imprecision for this point is consistently much higher than the other values.) Taken together these results show that the film sensitivity to O_2 is a strong function of the amount of $[Ru(dpp)_3]^{2+}$ sequestered within the film.

Time-Resolved Intensity Decay. If we consider the results presented in Figure 2 in terms of a simple Stern-Volmer scheme (eq. (1)), we can see that the average K_{SV} value must increase as the $[Ru(dpp)_3]^{2+}$ concentration in the film increases. Such a result could arise from increases in the mean $[Ru(dpp)_3]^{2+}$ excited-state luminescence lifetime in the absence of quencher ($<\tau_o>$), increases in the bimolecular quenching constant (k_q) or both.

To address this issue in more detail we performed a series of time-resolved luminescence experiments on the $[Ru(dpp)_3]^{2+}$-doped sol-gel-derived thin films to determine the effects of the $[Ru(dpp)_3]^{2+}$ concentration on the excited-

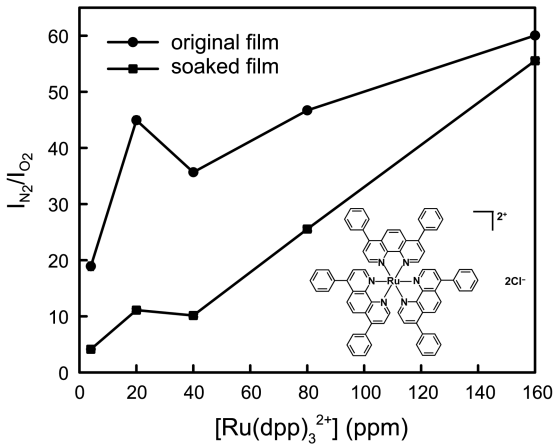

Figure 2. Effect of $[Ru(dpp)_3]^{2+}$ concentration on the film sensitivity to O_2 for original (●) and EtOH-soaked (■) films. Inset: Chemical structure of $[Ru(dpp)_3]^{2+}$.

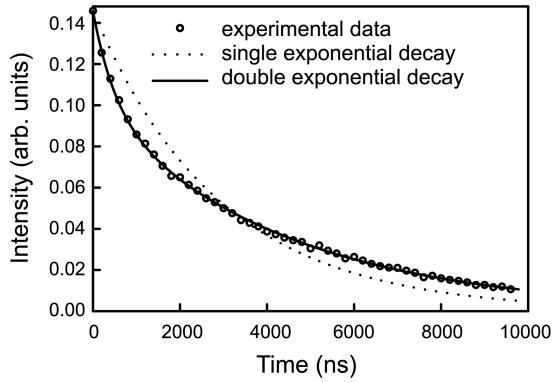

Figure 3. Typical excited-state intensity decay trace for a $[Ru(dpp)_3]^{2+}$-doped sol-gel-derived thin film under ambient processing conditions under N_2. Data (○) and fits to single (-------) and a double exponential (——) decay models.

state intensity decay kinetics. Figure 3 presents a typical data set (points) for a 400 μM $[Ru(dpp)_3]^{2+}$-doped film. (The full-width at half maximum for the instrument response function is on the order of 40 ns for our instrument.) Also shown are the fits between the experimental data and single (-------) and double exponential (———) decay models. One can clearly see that the single exponential decay model does not describe the data well. Similar results were always seen when the $[Ru(dpp)_3]^{2+}$ concentration was greater than or equal to 50 μM. Below ~50 μM $[Ru(dpp)_3]^{2+}$, the intensity decay is reasonably well described by a single exponential decay model.

The results presented in Figure 3 demonstrate that the $[Ru(dpp)_3]^{2+}$ decay kinetics at moderate to high $[Ru(dpp)_3]^{2+}$ concentrations is made up of the emission from two microdomains. In Figure 4(a) we present the average $[Ru(dpp)_3]^{2+}$ luminescence lifetime ($<\tau_o>$) as a function of the $[Ru(dpp)_3]^{2+}$ concentration within the film. These results show that the reason behind the change in I_{N2}/I_{O2} seen in Figure 2 is an increase in the average $[Ru(dpp)_3]^{2+}$ luminescence lifetime as the $[Ru(dpp)_3]^{2+}$ concentration increases.

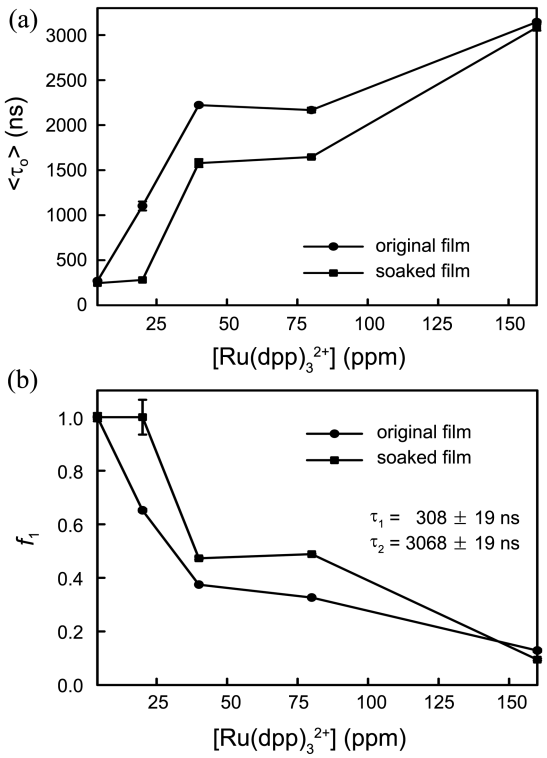

Figure 4. Effect of $[Ru(dpp)_3]^{2+}$ concentration on the average $[Ru(dpp)_3]^{2+}$ luminescence lifetime (Panel A) and the fractional contribution of the shorter-lived species (Panel B).

To address the origin of the change in the average $[Ru(dpp)_3]^{2+}$ luminescence lifetime in more detail we used a global analysis strategy[28] to simultaneously analyze all the intensity decay traces at all $[Ru(dpp)_3]^{2+}$ concentrations. The results of this exercise are summarized in Table 1. Inspection of Table 1 shows that the concentration-dependent $[Ru(dpp)_3]^{2+}$ intensity decay kinetics in the sol-gel-derived films can be described by a model wherein the $[Ru(dpp)_3]^{2+}$ is simultaneously emitting from two discrete microenvironments with intrinsic luminescence lifetimes of 308 ± 19 (τ_1) and 3068 ± 23 ns (τ_2) that are concentration independent. However, as the $[Ru(dpp)_3]^{2+}$ concentration in the film increases from

Table 1. Average[a] r^2 for the fits of the $[Ru(dpp)_3]^{2+}$ intensity decay data to various test models

Model	Total # of Floating Parameters[b]	r^2
Single Exponential	1	0.723
Double Exponential	3	0.901
Double exponential (τ_1 linked = 308 ± 19 ns)	2	0.901
Double exponential (τ_2 linked = 3068 ± 23 ns)	2	0.896
Double exponential (τ_1 linked = 308 ± 19 ns) (τ_2 linked = 3068 ± 23 ns)	1	0.900

[a]12 intensity decay traces are analyzed simultaneously. [b]refers to the number of floating parameters per data file (i.e., $[Ru(dpp)_3]^{2+}$ concentration).

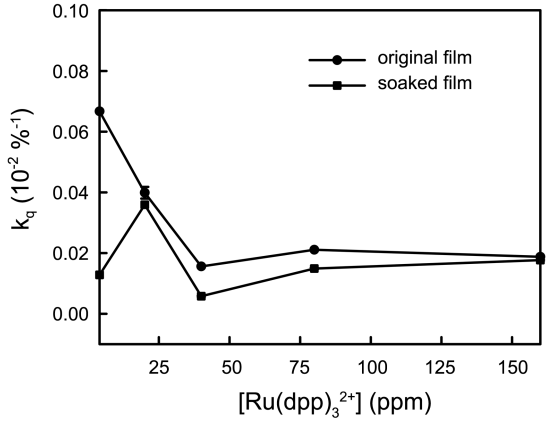

Figure 5. Effect of $[Ru(dpp)_3]^{2+}$ concentration on the recovered average bimolecular quenching constant for $[Ru(dpp)_3]^{2+}$-doped sol-gel-derived thin films.

3 to 400 μM, the fraction of the observed luminescence that is associated with the longer-lived species (τ_2) goes from essentially zero at 3 μM to over 90% at 400 μM $[Ru(dpp)_3]^{2+}$. For completeness, Figure 5 shows that the average k_q is independent of the $[Ru(dpp)_3]^{2+}$ concentration. This result argues that O_2 transport within the film per se is not the origin of the results seen in Figure 2. Thus, the sole reason for the changes in observed sensitivity (Figure 2) is associated with a change in the distribution of the $[Ru(dpp)_3]^{2+}$ molecules within the film with changes in the $[Ru(dpp)_3]^{2+}$ concentration.

A Model. Figure 6 presents a model that is consistent with our results. In this depiction, we focus on a single pore and the immediate environment that surrounds the pore. There are two possible locations for the $[Ru(dpp)_3]^{2+}$ molecules (●) within a TEOS-based xerogel: in the pore walls and on the pore surface. When the $[Ru(dpp)_3]^{2+}$ concentration is $\leq$ 50 μM, the $[Ru(dpp)_3]^{2+}$ molecules are mainly distributed inside the pore walls ($f_1 \sim 1$). This environment is such that the $[Ru(dpp)_3]^{2+}$ is heavily quenched ($\tau_1 = 308 \pm 19$ ns). As the $[Ru(dpp)_3]^{2+}$ concentration in the film increases, the $[Ru(dpp)_3]^{2+}$ molecules begin to simultaneously distribute into the pore wall and onto the pore surface. At the highest $[Ru(dpp)_3]^{2+}$ concentrations studied, the majority of the luminescence comes from those $[Ru(dpp)_3]^{2+}$ species ($f_2 >$ 0.9) that are simultaneously the most accessible to O_2 and

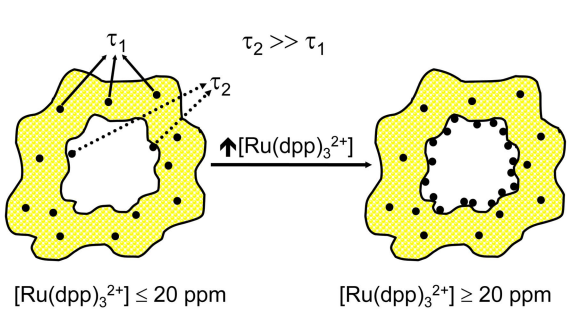

Figure 6. Model to describe the effects of $[Ru(dpp)_3]^{2+}$ concentration on the $[Ru(dpp)_3]^{2+}$ (●) distribution within the pore of sol-gel derived thin film. Note: Not drawn to scale.

the more sensitive to the presence of O_2 (e.g., τ_2 is ~10-fold greater than τ_1).

Conclusions

The sensitivity of $[Ru(dpp)_3]^{2+}$-doped sol-gel derived thin films to O_2 depends on the $[Ru(dpp)_3]^{2+}$ concentration in the film. The origin of this concentration-dependent change in sensitivity arises from the $[Ru(dpp)_3]^{2+}$ distributing simultaneously between two discrete microenvironments within the xerogel films. These environments are such that the $[Ru(dpp)_3]^{2+}$ excited-state luminescence lifetimes differ by an order-of-magnitude. Both environments are independent of the $[Ru(dpp)_3]^{2+}$ concentration; the only variable is a change in the fractional contribution of the $[Ru(dpp)_3]^{2+}$ species distributed within each environment. These results conclusively demonstrate that the dopant concentration can play a crucial role in the performance of devices based on sol-gel processing methods.

Acknowledgments. The authors thank Professor F.V. Bright at University at Buffalo-The State University of New York for discussions.

References

1. Ciriminna, R.; Carà, P. D.; Sciortino, M.; Pagliaro, M. *Adv. Syn. Cat.* **2011**, *353*(5), 677-687.
2. Liu, J. W.; Yang, Y.; Chen, C. F.; Ma, J. T. *Langmuir.* **2010**, *26*(11), 9040-9044.
3. Tran-Thi, T. H.; Dagnelie, R.; Crunaire, S.; Nicole, L. *Chem. Soc. Rev.* **2011**, *40*(2), 621-639.
4. Adamski, J.; Kochana, J. *Cent. Eur. J. Chem.* **2011**, *9*(1), 185-191.
5. Monton, M. R. N.; Lebert, J. M.; Little, J. R. L.; Nair, J. J.; McNulty, J.; Brennan, J. D. *Anal. Chem.* **2010**, *82*(22), 9365-9373.
6. Menaa, B.; Menaa, F.; Aiolfi-Guimaraes, C.; Sharts, O. *Int. J. Nanotechnol.* **2010**, *7*(1), 1-45.
7. Ahn, J. Y.; Jo, M.; Dua, P.; Lee, D.; Kim, S. *Oligonucleotides* **2011**, *21*(2), 93-100.
8. Si, Z.; Li, J.; Li, B.; Zhao, F.; Liu, S.; Li, W. *Inorg. Chem.* **2007**, *46*(15), 6155-6163.
9. Hamity, M.; Senz, A.; Gsponer, H. *J. Photochem. Photobiol. A-Chem.* **2006**, *180*(1-2), 9-14.
10. Lu, W.; Mi, B. X.; Chan, M. C. W.; Hui, Z.; Che, C. M.; Zhu, N.; Lee, S. T. *J. Am. Chem. Soc.* **2004**, *126*(15), 4958-4971.
11. Watkins, A. N.; Ingersoll, C. M.; Baker, G. A.; Bright, F. V. *Anal. Chem.* **1998**, *70*(16), 3384-3396.
12. Daivasagaya, D. S.; Yao, L.; Yung, K. Y.; Hajj-Hassan, M.; Cheung, M. C.; Chodavarapu, V. P.; Bright, F. V. *Sensor. Actuat. B-Chem.* **2011**, *157*(2), 408-416.
13. Navarro, R. M.; Alvarez-Galván, M. C.; de la Mano, J. A. V.; Al-Zahrani, S. M.; Fierro, J. L. G. *Ener. Environ.Sci.* **2010**, *3*(12), 1865-1882.
14. Grist, S. M.; Chrostowski, L.; Cheung, K. C. *Sensors* **2010**, *10*(10), 9286-9316.
15. Carraway, E. R.; Demas, J. N.; Degraff, B. A. *Anal. Chem.* **1991**, *63*(4), 332-336.
16. Carraway, E. R.; Demas, J. N.; Degraff, B. A.; Bacon, J. R. *Anal. Chem.* **1991**, *63*(4), 337-342.
17. Lin, C.; Böttcher, W.; Chou, M.; Creutz, C.; Sutin, N. *J. Amer. Chem. Soc.* **1976**, *98*(21), 6536-6544.
18. Ener, M. E.; Lee, Y. T.; Winkler, J. R.; Gray, H. B.; Cheruzel, L.

Proc. Nat. Acad. Sci. **2010**, *107*(44), 18783-18786.
19. Wu, X.; Song, L.; Li, B.; Liu, Y. *J. Lumin.* **2010**, *130*(3), 374-379.
20. Ji, S.; Wu, W.; Song, P.; Han, K.; Wang, Z.; Liu, S.; Guo, H.; Zhao, J. *J. Mater. Chem.* **2010**, *20*(10), 1953-1963.
21. Matthews, L. R.; Wang, X. J.; Knobbe, E. *Mater. Res. Soc. Symp. Proc.* **1994**, *329*, 285-285.
22. Baker, G. A.; Wenner, B. R.; Watkins, A. N.; Bright, F. V. *J. Sol-gel Sci. Technol.* **2000**, *17*(1), 71-82.
23. Lakowicz, J. R. *Principles of Fluorescence Spectroscopy*, 3rd ed.; Springer: New York, 2006.
24. Bonzagni, N. J.; Baker, G. A.; Pandey, S.; Niemeyer, E. D.; Bright, F. V. *J. Sol-gel Sci. Technol.* **2000**, *17*(1), 83-90.
25. Xu, W.; Schmidt, R.; Whaley, M.; Demas, J. N.; DeGraff, B. A.; Karikari, E. K.; Farmer, B. L. *Anal. Chem.* **1995**, *67*(18), 3172-3180.
26. Jordan, J. D.; Dunbar, R. A.; Bright, F. V. *Anal. Chem.* **1995**, *67*(14), 2436-2443.
27. Demas, J.; DeGraff, B. *J. Chem. Edu.* **1997**, *74*(6), 690-695.
28. Beechem, J. M.; Brand, L. *Annu. Rev. Biochem.* **1985**, *54*, 43-71.